Hindawi
International Journal of Photoenergy
Volume 2021, Article ID 9956433, 19 pages
https://doi.org/10.1155/2021/9956433

Research Article

A Novel Experimental and Approach of Diagnosis, Partial Shading, and Fault Detection for Domestic Purposes Photovoltaic System Using Data Exchange of Adjacent Panels

H. A. Raeisi and S. M. Sadeghzadeh

Shahed University, Faculty of Engineering, Khalig-e-Fars Freeway, Tehran, Iran 18155/159, 3319118651

Correspondence should be addressed to S. M. Sadeghzadeh; sadeghzadeh@shahed.ac.ir

Received 1 April 2021; Revised 25 July 2021; Accepted 20 August 2021; Published 18 September 2021

Academic Editor: Elias Stathatos

This paper presents a new detection method of fault and partial shading condition (PSC) in a photovoltaic (PV) domestic network, considering maximum power point tracking (MPPT). The MPPT has been executed by employing a boost converter using particle swarm optimization (PSO) technique. The system is composed of two photovoltaic arrays. Each PV array contains three panels connected in series, including distinct MPPT. The PSC detection exploits the neighboring PV system data. This suggested innovative algorithm is proficient in detecting these subjects: (a) fault, (b) partial shading condition, (c) solar panel (d) panel's relevant bypass diode failure, (d) converter failure alongside specifying the failed semiconductor, and (e) PV disconnection failure. The simulation process has been implemented using MATLAB/Simulink software. To this end, the proposed method was investigated experimentally using two 250 W PV solar set under various PSCs and faults. A data exchange link is used to implement an integrated management system. The Zigbee protocol was also chosen to data exchange of converters. The results validated the applicability and practicality of this algorithm in domestic PV systems.

1. Introduction

Photovoltaic (PV) energy systems are considered as promising renewable energy production systems compared to other conventional energy sources such as natural gas, fossil fuels, and coal [1], and a large body of research exists on extracting maximum power from these systems. MPPT can lead to increased efficiency in applications such as domestic power supply, solar water pumps, and hybrid energy systems including photovoltaic.

Various techniques are suggested for tracking the maximum power point (MPP) of PV energy systems under variable environmental conditions. MPPT techniques are usually capable of tracking MPP under uniform solar radiation. However, these techniques do not guarantee to track accurate MPP under partial shading conditions [2]. Partial shading (PS) is a very frequent phenomenon which may adversely affect the P-V characteristic curve of PV arrays [3, 4]. It occurs when some parts of the cells or modules of the PV system are shaded due to damage, dust, trees, moving clouds during the day, or adjacent buildings and towers. Shaded PV modules negatively affect the power output and overall efficiency of the PV system [4]. To overcome the undesirable effects of PS on PV arrays, various MPPT3 techniques such as MPPT estimation [5], iterative analytical method [6], FLC [7], ANFIS [8], PSO [9], FPSO [10], ANFIS-PSO [11], GA [12], Firefly algorithm [13], and modified sine-cosine method [14] are designed.

1.1. Literature Review. Most of the research on partial shading has focused on novel approaches to locate the real maximum power point under partial shading conditions and few have studied detection of partial shading occurrence.

1.1.1. Partial Shading. Ahmad and Salam (2016) suggested an accurate detection scheme for the occurrence of partial shading [15]. In this technique, two designed points on the I-V curve and the currents recorded for calculation of irradiance, i.e., G1 and G2, were scanned. Furthermore, the suggested method could be utilized to update the open-circuit voltage using the data obtained from these two scanned points, thus, eliminated the use of temperature and irradiance sensors. This led to lower cost and complexity of system implementation. Also, it enhanced the transient efficiency of MPPT by 30-35%.

Kaced et al. (2017) presented an MPPT method for PV systems under partial shading conditions using Bat Algorithm [16]. To evaluate the performance of the suggested method, several simulations were performed in Matlab/Simulink for various shading patterns. The algorithm was tested in real-time using a Buck-Boost converter and real PV panels. Results indicated that the suggested scheme outperformed P&O and PSO techniques in terms of accuracy and PV voltage fluctuations in transient time. In addition, experimental results supported the efficiency of this method for tracking the global peak and its high accuracy in addressing partial shading.

Ishaque et al. (2011) suggested very precise modeling of partial shading in PV system [17]. The major part of their work included the utilization of two diodes to represent the PV cell. The proposed model supported simulation of large-scale PV systems that could act as an interface between MPPT algorithms and real power electronic converters. In addition, this PV system was simulated along with power converters and controllers. The proposed model was compared with three other models, namely, artificial network, P&O, and single-diode model. Results indicated better performance of double-diode model compared to Rp and Rs models. It was predicted that the work would be of interest to people interested in designing a PV system and who need a simple, fast, and accurate PV model.

In a new approach, Betanzo et al. (2018) presented a PV-based DC microgrid that provided a high-quality bus voltage regulation in islanding mode, without being affected by partial shading or other problems due to PV module connection and disconnection [18]. In addition, it could prevent partial shading stress through disconnecting affected modules. Another advantage of the method included higher flexibility to connect more PV modules. It should be mentioned that the advantages of this approach were verified by a 200 W prototype.

MPPT is used to maximize power extraction from PV modules and feeds the power through a buck-boost converter that increases the voltage gain if required. In their project, Gokilapriya and Banu (2014) conducted an in-depth analysis of the concept of DPSO algorithm under partial shading conditions which significantly increased the PV system efficiency [19]. To evaluate this idea, the algorithm was applied to the buck-boost converter and compared to the conventional PSO method. DPSO and PSO methods along with P&O technique were presented for tracking MPP of a PV system. This project showed that a DC/DC converter of the buck-boost type was capable of tracking maximum power point of a PV panel at all times, regardless of cell temperature, solar radiation, and connected load.

Farzaneh et al. (2018) presented a modified firefly algorithm for tracking the maximum power point under partial shading conditions [20]. The performances of the proposed and existing PSCs-based methods were studied in MATLAB/Simulink software. Simulation results indicated that the proposed method, FA, and PSO were capable of tracking GMPP under partial shading condition (PSC). Also, the speed of this approach in tracking GMPP under PSC was higher than that of FA and PSO. Higher speed and efficiency were among the advantages of the proposed method, and its average efficiency was more than 99.98%.

In a research project, Vijayalekshmy et al. (2014) compared the performance of two arrays connected in series and parallel modes having three modules at different angles of partial shading [21]. Modules were connected in series to meet the desired voltage. Under partial shading, however, various significant losses occurred which led to an evident decrease in the fill factor (FF). Therefore, it was concluded that, for low-power schemes, parallel-connected short strings were more suited than series-connected ones.

Martin et al. (2018) presented a new approach for deriving MPP under partial shading using artificial vision [22]. In the artificial vision approach, a webcam is used to identify the shadow irradiance in real-time and to provide the reference voltage that supplies the maximum power regardless of the number of peaks in the P-V curve. Then, the reference voltage is used by a robust and nonlinear control, back stepping controller, for regulating the input voltage of the DC/DC converter to assure the maximum power output of PV modules. The validity of the proposed method in increasing the MPP tracking efficiency from 98.1 to 99.6% was verified by experimental tests carried out in outdoor space.

Many of the reviewed papers have focused on finding the true maximum power point, and only a few have addressed the shading detection which their proposed methods do not have the desired efficiency due to their computational load and unusual accessories needed like camera. This study develops a novel approach for partial shading condition and fault detection based in adjacent panel information.

1.1.2. Fault Detection. Faults and errors may happen in all parts of a PV system, such as PV arrays, transmission cables, controller system, converters, inverters, and batteries. Shutting down the PV generation system under different fault conditions eliminates the reliability and continuity of power generation. A study in 2010 showed that faults have a potential effect on reducing the power generated by a PV system annually by about 18.9% [23]. Therefore, it was essential to develop proper techniques which can that detect faults in PV system to maximizing the operational performance and reliability of the overall system.

System failures are divided into two categories, DC side and AC side of which only DC side fault has been studied in this article.

Types of DC faults that might occur in a PV system include mismatch faults, asymmetrical fault, ground fault, arc fault, bypass diode and open circuit faults, lightening, DC-DC converter fault, and energy storage [24].

Chouder and Santiago (2010) present a new automatic supervision and fault detection procedure for PV systems, based on the power losses analysis. This automatic supervision system has been developed in Simulink software and tested experimentally [25].

In a new approach, Pillai and Natarajan (2018) presented a fault detection method, MPPT-based sensor less line—line and line—ground. The proposed method can also detect partial shading and error occurrence in low radiation [26].

Jamshidpour et al. (2019) suggested a Unified Switch Fault Diagnosis (UFD) approach for two-stage nonisolated DC-DC converters used in energy harvesting applications which is simpler than the two parallel fault diagnosis methods in realization. Moreover, it can detect both types of switch failures: open circuit and short circuit switch faults [27].

Khalil et al. (2020) conduct comparative analysis of PV faults, and performance evaluation of its detection techniques has been carried out. PV error not only reduces output power and efficiency but also affects systems' lifetime. In their work, variety of errors are investigated and researched based on the PV mathematical model [28].

Ahmad et al. (2021) presented a fault diagnosis for an interleaved boost converter in a PV-based system. The effect of open-circuit fault of each semiconductor on the PV system converter has been investigated [29].

Most of the reviewed papers have focused on one of the possible errors. The novel approach of the present work can identify more faults. First, the proposed method is described and, after implementation, the obtained results are studied and discussed.

1.1.3. Features of PV Array under Partial Shading Condition. There are two methods for modeling solar cell: one-diode model and two-diode model which are depicted in Figure 1, respectively. In this paper, a one-diode solar panel model is used for PV simulation [30].

Power output (I) and voltage (v) can be described as the following formula:

$$I_L = I_{sc}\left[1 - C_1\left(e^{V_L/C_2 V_{oc}} - 1\right)\right]. \tag{1}$$

The mathematical relation governing the solar cell under STC conditions is as follows:

$$\begin{aligned} C_1 &= \left(1 - \frac{I_m}{I_{sc}}\right)e^{-V_m/C_2 V_{oc}}, \\ C_2 &= \left(\frac{V_m}{V_{oc}} - 1\right)\left[Ln\left(1 - \frac{I_m}{I_{sc}}\right)\right]^{-1}, \end{aligned} \tag{2}$$

where I_L is the panel's current, V_L is the panel's output voltage, V_{oc} is the open-circuit voltage, I_{sc} is the short circuit current, and V_m, I_m are voltage and current of panel's maximum power point. The value of model parameters under non-STC condition can be obtained by the following relations [31]. Time coefficient of thermal voltage also can be calculated by following formula:

$$\begin{aligned} I'_{sc} &= I_{sc}\frac{S}{S_{\text{ref}}}(1 + \alpha\Delta T), \\ I'_m &= I_m\frac{S}{S_{\text{ref}}}(1 + \alpha\Delta T), \\ V'_{oc} &= V_{oc}\frac{S}{S_{\text{ref}}}(1 - \gamma\Delta T)\text{Ln}(1 + \beta\Delta S), \\ V'_m &= V_m\frac{S}{S_{\text{ref}}}(1 - \gamma\Delta T)\text{Ln}(1 + \beta\Delta S), \end{aligned} \tag{3}$$

where α, β, and Υ are constant values representing parameters' variability due to changes in temperature and irradiation. Given the values of these coefficients, the effect of temperature variations can be overlooked by a good approximation.

Each panel is typically composed of a number of cells connected in series to increase the total voltage. In this series combination, in case of lower current of a cell due to being nonuniformly illuminated or using cells with various specifications, local overheating or "hot spots" are formed which result in lower production, efficiency, and lifetime of panel. Bypass diodes are used to solve the problem of hot spot heating. There are three of them in parallel with one-third of the solar cell array each. When part of the panel is in partial shading condition and its current is lower than other parts, the corresponding bypass diode goes to "bypass" mode and prevents the related problems, however, the panel's I-V curve may show multiple steps and the P-V curve may exhibit multiple local maxima.

Given the fact that equation (1) is derived for uniform illumination conditions, it is not applicable for partial shading conditions. In this situation, the curve is divided into two parts due to the performance of bypass diode in partially shaded string [31]: in the first part, the current of strings under uniform illumination is higher than the current of strings under shading, so the diode "bypass" mode activates. The equation governing the panel in this condition can be written as follows:

$$I_L = I_{sc}\left[1 - C_1\left(e^{V_L/C_2 V_{oc}(m/m+n)} - 1\right)\right], \tag{4}$$

where m is the number of equally illuminated strings. When the current of these two strings is equated, diode goes to "off" mode and, from this point on, the current magnitude is controlled by partially shaded strings. This can be shown by:

$$I_{\text{L}} = I_{sc}\left[1 - C_1\left(e^{V_L - V_s/C_2 V_{oc}(n/m+n)} - 1\right)\right], \tag{5}$$

where n is the number of partially shaded strings and V_{s} is the shadowed cell voltage. By calculating V_s via equating these two equations, the above equations can be rewritten as the following equation system to model the panel:

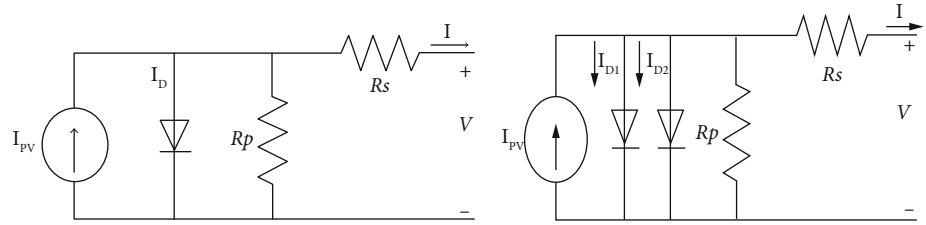

(a) Single diode model (b) Two diode model

Figure 1: One and two diode model of solar cell.

$$I_L = I_{sc}\left[1 - C_1\left(e^{V_L/C_2V_{oc}(m/m+n)} - 1\right)\right] V_{sc} \le V_L \le V_s,$$
$$I_L = I_{sc}\left[1 - C_1\left(e^{V_L - V_s/C_2V_{oc}(n/m+n)} - 1\right)\right] V_{oc} \ge V_L > V_s, \quad (6)$$

where V_{SC} is short circuit voltage of the panel. Table 1 shows the value of the parameters used in the simulated photovoltaic model.

The current-voltage characteristic curve of this simulated model at $25^{\circ C}$ and in different radiations is shown in Figure 2.

As seen in Figure 2, with an increase in sunlight radiation, both current and voltage increase, thus, according to this rise, the photovoltaic output power will increase consequently. It is worth mentioning that with zero radiation, there is output voltage but not current, which means in partial shading conditions which a panel's output power is zero, current is zero, but not voltage. Figure 3 shows what would happen to current, if a panel's output power tends to zero. The red line is the current path.

To reduce shading effects, bypass diodes are mounted on each panel, and blocking diodes are installed on each PV string [32, 33]. Figure 2 illustrates V-I curves for each of these conditions. As seen, there is a significant difference between these three states with multiple local peaks for the shaded region and only a single peak for normal condition.

Figure 4 shows three characteristic curves of a PV system, assuming constant temperature, and Table 2 shows the varied radiances of panels.

Given the remarkable decline in panel's power output under partial shading conditions and the importance of its determination for deriving a new operating point to gain the maximum power, it has always been important to determine whether partial shading has occurred. A boost converter helps this algorithm to track the maximum power of PV. Figure 5 shows the block diagram of the boost converter.

In converter-based and other conventional MPPT methods, after a given period of time, the algorithm is implemented again to locate a new MPP. If no shadows, faults, or changes in irradiance occur, the implementation of this algorithm reduces the panel's power output and consequently the system's efficiency. On the other hand, in the time interval between two implementations, the panel may be under partial shading condition or fault, which reduces the power

Table 1: Simulated panel characteristic.

Open circuit voltage	40 v
Short circuit current	10 A
MPP voltage	33 V
MPP current	9.5 A

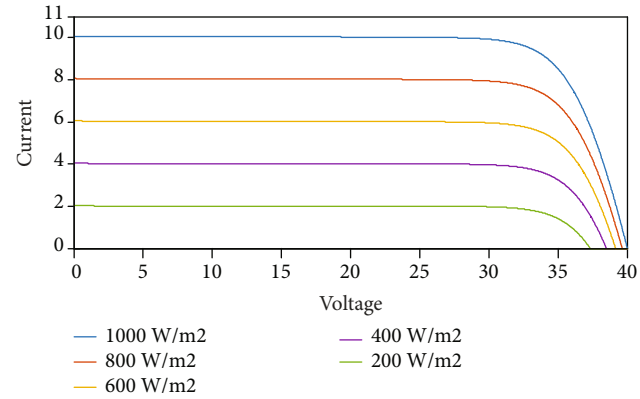

Figure 2: The current-voltage characteristic curve of PV model.

output compared to the maximum power available and thus lowers the efficiency. Conventional algorithms such as P&O, INC. CON., and Hill Climbing cannot discriminate between GMPP and LMPP points, and they may mistakenly stop at a local point. To overcome this problem, other more advanced algorithms like PSO are used which are capable of finding the true point at the cost of more complex and, at times, more prolonged implementation and thus lower efficiency. PSO algorithm has the advantage of operating independently. Most of the other methods are not capable of accurately tracking MPP where the radiation levels change speedily.

However, under uniform irradiance, these methods are not needed. If the occurrence of partial shading can be detected, individual algorithms appropriate for uniform irradiance and partial shading can be used.

Solar energy is widely used for domestic applications using various topologies [30]. The topology of this paper configuration is shown in Figure 6. In this configuration, each converter

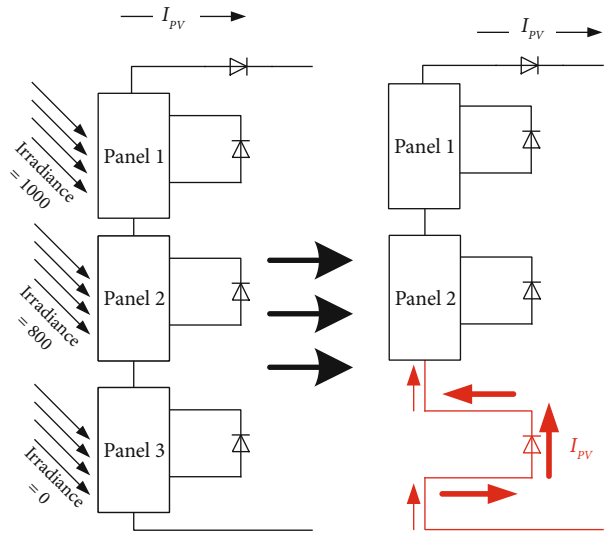

Figure 3: The current path in zero radiation condition of a panel.

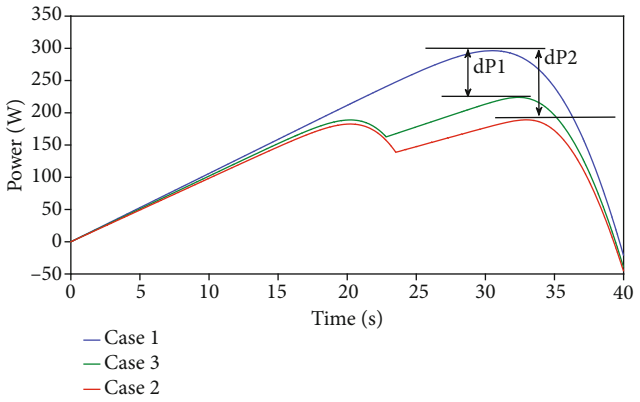

Figure 4: P-V characteristic curves for uniform irradiance and partial shading conditions.

implements the MPPT algorithm individually for the PV system to which it is connected. In this topology, under uniform radiation, all panels usually have rather equal operating point voltages and power outputs.

2. The Proposed Method

Since partial shading occurs on some panels, the power output of the former is reduced. By comparing the power output of each PV system with that of other one, provided that there is a significant difference between powers, the occurrence of partial shading can be detected. Assuming uniform irradiance $1000w/m^2$, if the panel's operating point corresponds to the maximum power point and panel undergoes partial shading without changing the operating point, the power output of panel will significantly reduce which is shown in Figure 4.

Table 2: Varied radiances of panels.

Item	Panel 1	Panel 2	Panel 3	Unit
Case 1	1000	1000	1000	w/m^2
Case 2	1000	1000	600	w/m^2
Case 3	1000	1000	700	w/m^2

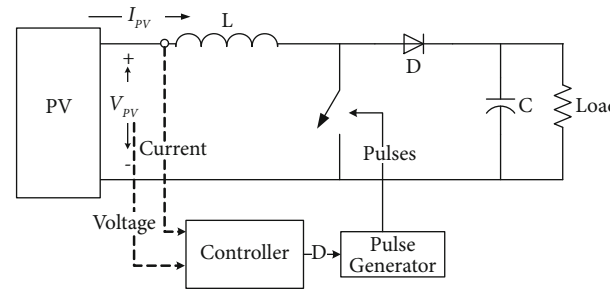

Figure 5: The block diagram of the boost converter.

By comparing the power of panels, in case of significant difference in the power of one or number of panels without any change in voltage, it can be concluded that those panels have been under partial shading condition. Given fast detection of partial shading in this method and transient nature of some partial shadings, the conditions are evaluated again shortly after some partial shading is detected and in case of continual partial shading, the appropriate algorithm is implemented, while for uniform radiation during longer time intervals, a typical algorithm is implemented for finding a new operating point that corresponds to the new uniform radiation.

The most outstanding merit of this proposed method is the elimination of programing complexity for detection of faults and PSC. Other proposed methods in different literatures are almost complicated; however, the one which is proposed in this paper is not only simple but also very practical. The proposed algorithm is using PSO method for MPPT. In this case, PSC is detected rapidly and PSO will perform the essential functions in order to track the maximum power point.

As mentioned above, panels output power differences are compared with each other to detect PSC. Just in one case, it is probable that all six panels affected by PSC; hence, no power difference is detected. This condition might happen rarely, and a solution is considered for it. If each panel is in PS condition, the panel receives less radiation, thus, in specific time during a day, there would be a situation that PV output power is zero. Despite the continuity of sun radiation, there is no power output. Therefore, algorithm shows PSC for all panels.

In this paper, assumption is based on a failure in a panel of PV1, and consequently, the algorithm is set to detect failure or PSC. When a panel fails, it detaches from the circuit and the bypass parallel diode is in charge of current flow, and if there would be a failure in this diode, it will short the circuit. Where there is "=" sign in algorithm some

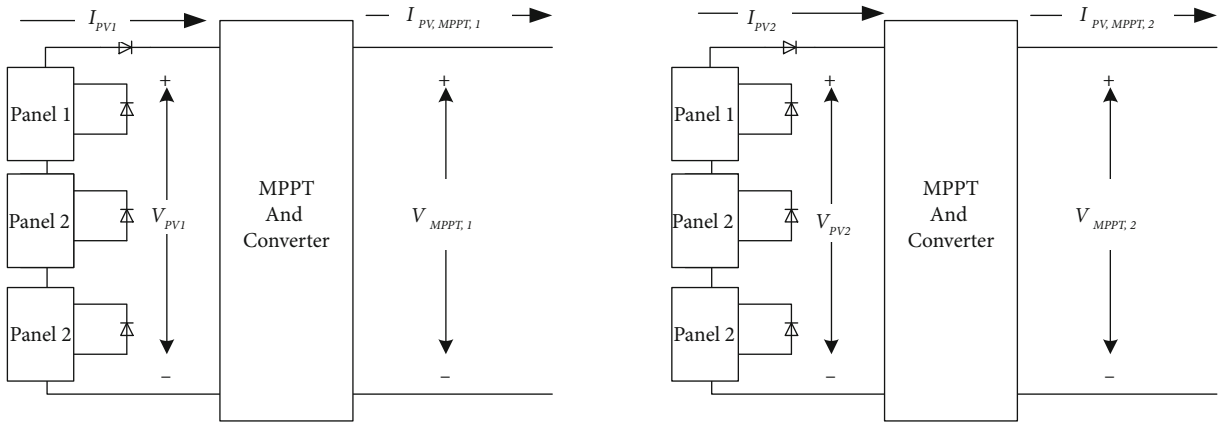

Figure 6: Domestic solar system configuration of this article.

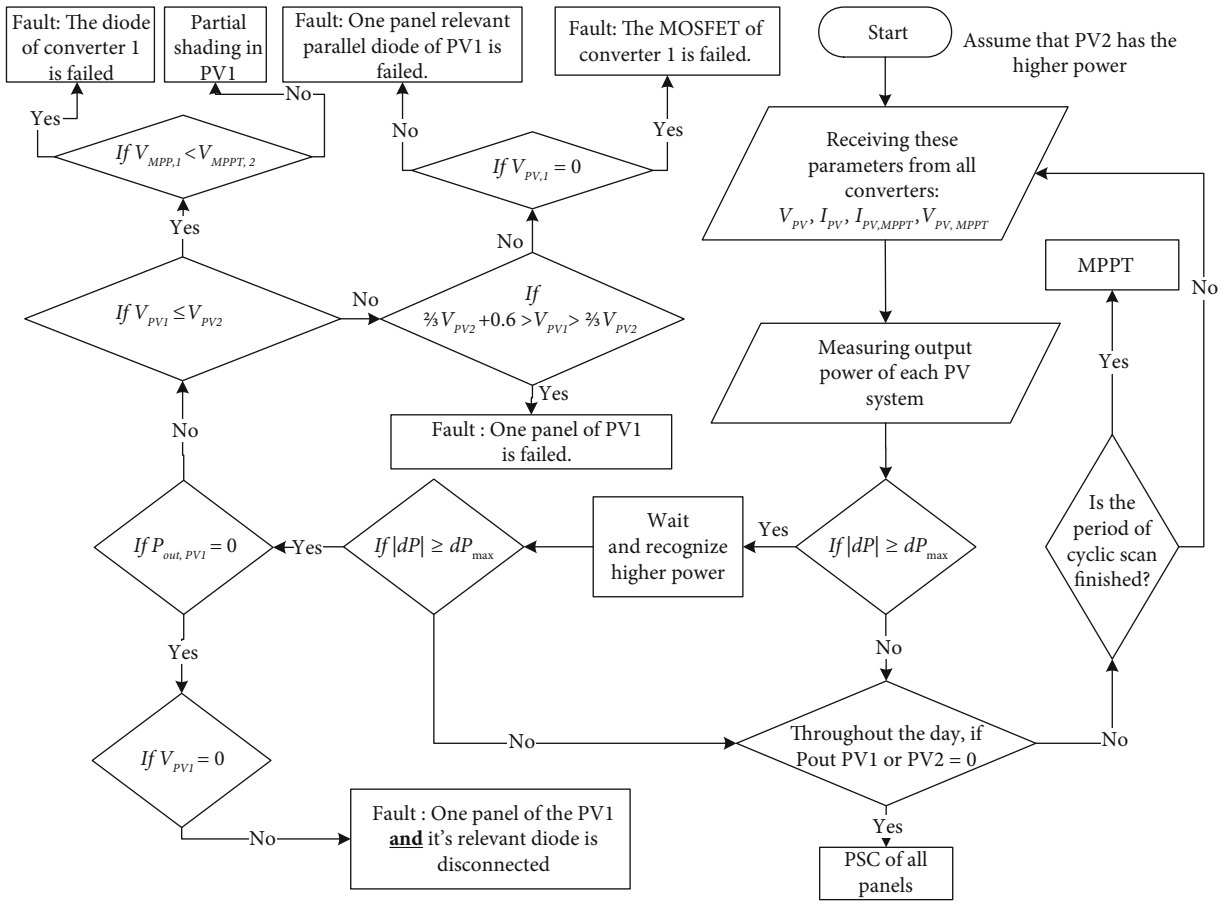

Figure 7: Flowchart of the proposed algorithm.

tolerance must be taken into account while programing. In fact, the sign of "=" meaning that both features have almost the same value.

In the previous section, fault and partial shading detection was discussed, and some related new articles were reviewed. The focus of this study is to accurately detect the faults or PSC. One of the advantages of this proposed method is using the low-cost sensors. In this algorithm, there is no need for high-precision voltage and current sensors and, in terms of cost, compared to a PV cell or a converter, it is economy. The required accuracy of the voltage sensor is about 0.1 volts. The used voltage sensor is

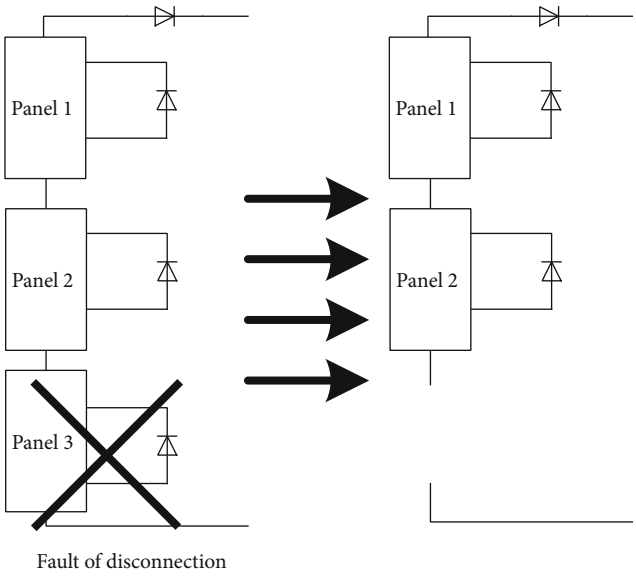

Figure 8: Disconnecting of a PV panel and the relevant bypass diode.

two parallel series resistors measuring the voltage by entering lower resistor's voltage into the microcontroller. The accuracy required to measure current is also about 0.1 amperes. Figure 6 shows the schematic of panel arrangement and the sampling location of the voltage and current parameters. It is assumed that an error has occurred in the photovoltaic system number one, and the algorithm intends to find the fault or PSC. For the simplicity of understanding this algorithm, the power of the PV1 system is considered less, and the diagnosis is made by creating various faults on panel number 3. By generalizing this algorithm to examine and compare all PVs, and implement this method in a matrix, fault detection for the entire system is provided. To fully understand the high performance of the algorithm, simplification has been used and all comparisons are made assuming a fault occurs in the first system.

2.1. Fault and Partial Shading Detection Algorithm. The algorithm used in this method is shown in Figure 7. The algorithm can be described as:

(a) Measuring the voltage and current parameters of PV and converter

(b) Calculating the power of each PV

(c) Comparing the power difference $|dP| \geq dP_{\max}$

(d) Measuring and comparing the output voltages of PVs

The algorithm will not start if the output power difference between the two photovoltaic systems is less than a certain value, and this value is called the $dP_{\max}$ power difference. Here, $dP_{\max} = 100\,\text{W}$ is considered. When the output power difference between the two photovoltaic systems exceeds 100 watts, after 10 second, the measured power output difference is compared with $dP_{\max}$. If this difference still exists, the next steps will continue. The reason for this waiting is that the factor which caused this difference may be resolved quickly. While system is faced PSC or fault, power difference remains constant, but if a power difference is observed for other reasons, the power difference may decrease after remeasurement and no diagnosis is required. If there is still a power difference, the output power of PV1 will be checked. If this power is zero or near zero, the output voltage of the string panels of PV1 is checked again. If the voltage is almost zero, it means that one of the PV1 panels and the bypass diode are completely disconnected from the circuit. Figure 8 shows the disconnection of the PV1 third photovoltaic panel and the relevant bypass diode.

If the output power of the PV1 system is not zero, the V_{PV1} voltage is compared with V_{PV2} .Then if $V_{PV1} \leq V_{PV2}$ and the output voltage of converter 1 is less than the output voltage of converter 2 ($V_{MPPT,1} < V_{MPPT,2}$), accordingly, the diode of converter1 is failed, otherwise, the PSC has occurred. Figure 9 shows the diode failure in converter.

A failed diode usually becomes short [33, 34]. When the switch is closed, capacitor C will be short-circuited and the converter output voltage will be dropped to zero, and as the switch is opened, the input voltage will be connected to the output. Figure 10 shows the switch opening, and Figure 11 shows the switch closing. It should be noted that with each duty cycle, when a pulse applies to the switch, the output voltage of the converter is finally zero, and if the controller does not command the switch to be close, the switch remains open, thus, the converter output voltage will not increase and will be equal to the input voltage.

If $V_{PV1} \leq V_{PV2}$, it is necessary to check the voltage. If $2/3V_{PV2} + 0.6 > V_{PV1} > 2/3V_{PV2}$, this means that one of the panels of PV1 has been failed. Figure 12 illustrates this situation. The forward voltage of diode in this situation is approximately 0.55 V.

Otherwise, the input voltage of converter 1 should be checked. If this voltage is approximately zero, it means that the MOSFET which used in converter 1 has been failed. Figure 13 demonstrates this situation. It is worth mentioning that usually when a MOSFET fails, it will become short [35–38].

If this voltage does not meet any of the above conditions, it means that one of the bypass diodes of PV1 panels has been failed. Figure 14 shows this situation.

In this method, each converter needs the information of other converters; therefore, a link for the exchange of data between converters is required.

3. Data Exchange

For the exchange of data between converters, a connection link is required. This link can be set up using wires or through a wireless connection. The wired connection can be implemented by such methods as PLC, I2C, and serial, while available communication protocols and radios can be utilized for wireless connection. In a wired connection, the system complexity increases due to using multiple wires

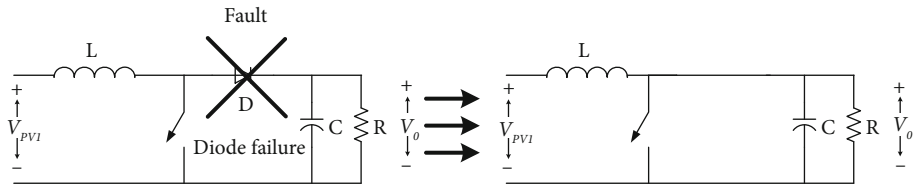

Figure 9: The diode failure in converter.

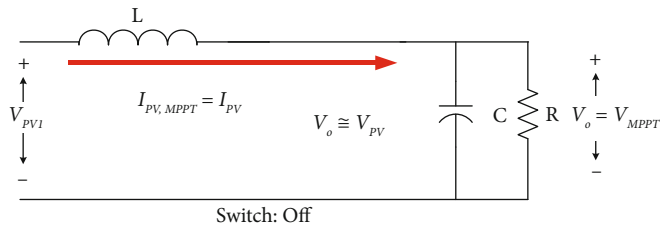

Figure 10: The circuit when the switch is open.

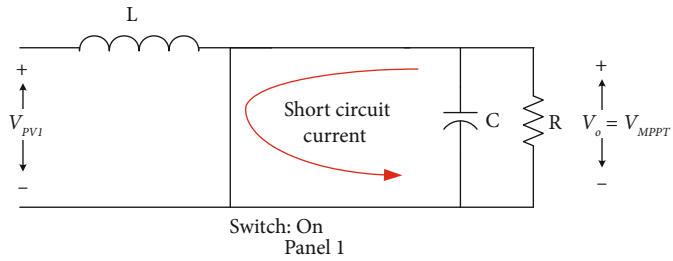

Figure 11: The circuit when the switch is open.

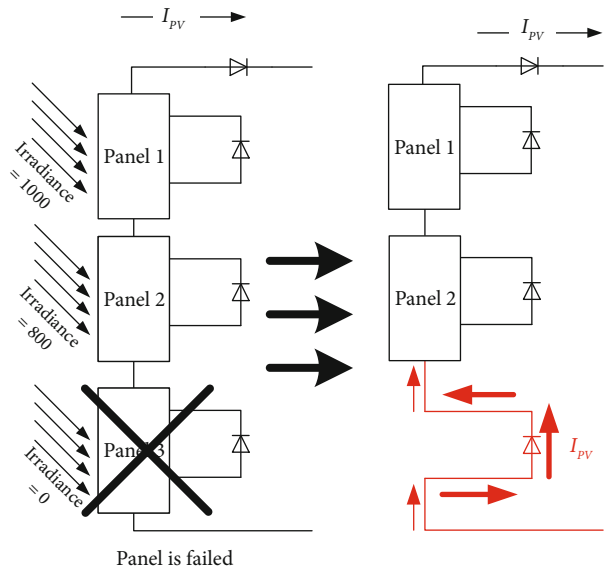

Figure 12: The third panel of PV1 is failed.

for implementation and also possible failure or disconnection of the link. This can lead to lower reliability and higher maintenance and repair costs. While the wireless mode does not suffer from these deficits. Therefore, the wireless method is selected in the present work.

The wireless connection should have the following characteristics:

(1) It has to be addressable for the exchange of data between specific converters, if necessary

(2) It shall provide simultaneous connection of multiple converters

(3) It shall allow the converters to be used as media for the exchange of data, if necessary

(4) It has to have reasonable security

Given the aforementioned features, Zigbee protocol was selected for the connection of converters. Zigbee is an IEEE 802.15.4-based standard used as a wireless sensor and control network suitable for low-rate of data transmission. Due to using 128-bit symmetric encryption, this protocol provides an adequate level of security. Using this protocol, Star, Peer to Peer, and Mesh topology can be implemented by a maximum number of 25 nodes per network. Zigbee

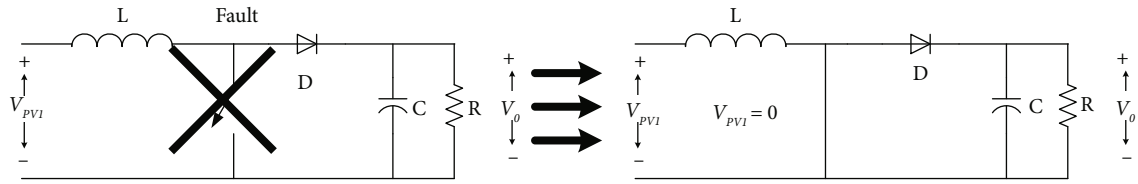

Figure 13: MOSFET failure in converter.

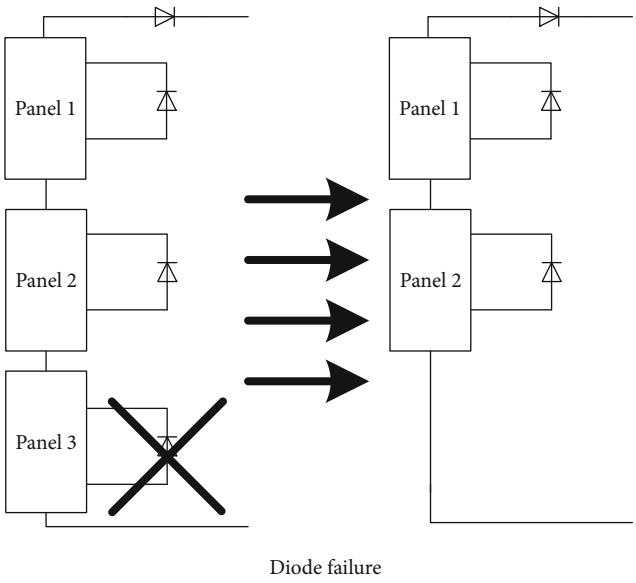

Figure 14: A panel bypass diode's failure.

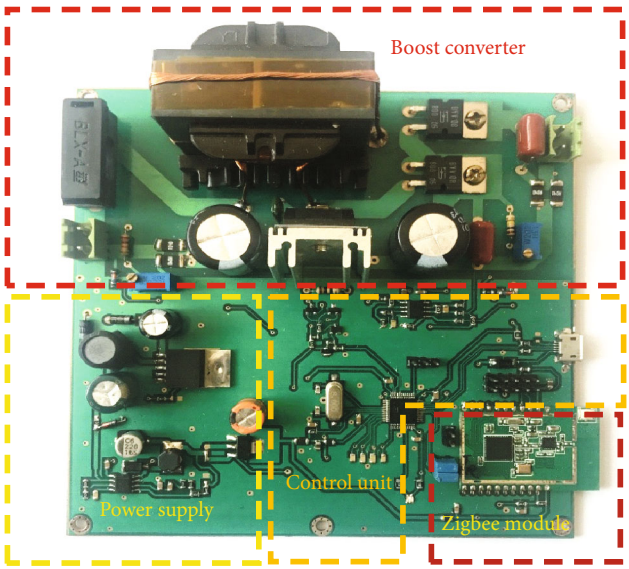

Figure 15: Boost converter.

chips are typically integrated with radio and microcontrollers embedded in a module. Zigbee devices are categorized into three types of coordinator, full function, and reduced function.

Table 3: Boost converter specifications.

Item	Value	Unit
Capacitor	100	μF
Inductor	220	μH
Switching frequency	100	kHz

Coordinators are used for network control and communication with other networks, and they are capable of storing network data. Each network requires a coordinator. FFD is an intermediary router that transfers and passes data among the devices. RFD is capable of transmitting and receiving data.

Given these facts, the Zigbee chip in one converter plays a coordinator role, and the rest is used for the exchange of data.

A wide range of data including voltage, current, power, and duty cycle can be transmitted, and the exchange of data occurs in accordance with the desired application. The aim of data transmission is to know the status of other converters and to use the data transmitted for improving the converter's performance.

To this end, all the converter's data or part of it that is adequate for the abovementioned purposes can be transmitted. Transmission of whole data causes higher power consumption by radio, longer transmission times, and assignment of more controller time to data processing. Therefore, it seems more reasonable to transmit only those data that are required for the aforesaid purposes. Since the aim of data transmission in the present work is to detect the occurrence of shadows or partial shading that adversely affect the power output and operating point voltage of the converter and panel, this goal can be achieved by transmitting the data about voltage and operating point power.

4. Implementation

To validate the simulation, a boost converter is designed that is shown in Figure 15 and specified in Table 3.

The data exchange link has been implemented using CC2330PA1 module with a CC2530 chip.

In this set, an STM32-series ARM microcontroller is employed for converter control, exchange, and utilization of data. Figure 16 indicates the general structure of the converter.

For the purpose of uniformity and controllability of experimental conditions, a solar panel simulator [31], whose

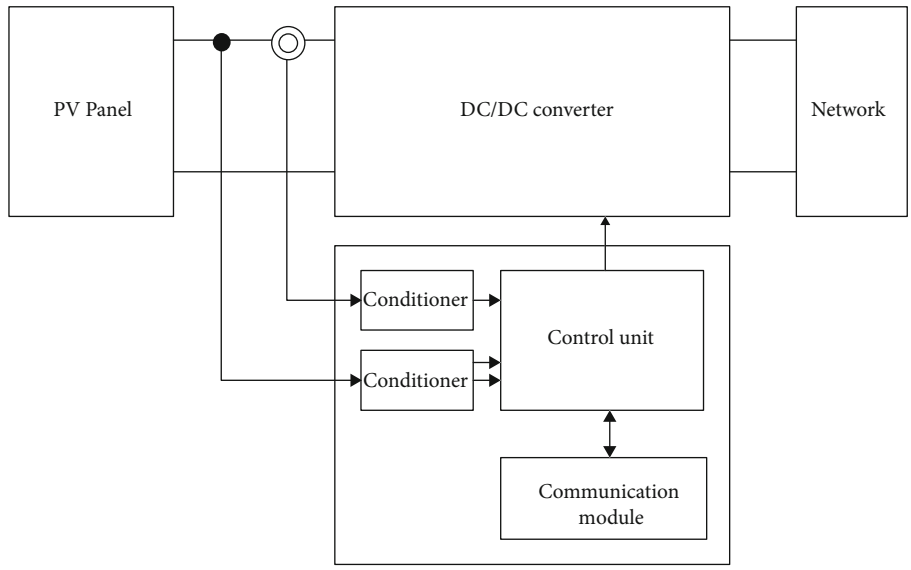

Figure 16: General structure of the converter.

Table 4: Measured electrical characteristic of constructed panel simulator.

Item	Value	Unit
V_{oc}	40	V
I_{sc}	8.62	A
V_{mpp}	30.8	V
I_{mpp}	8.1	A

specifications are given in Table 4, is used for the converter input assuming constant temperature. Figure 17 represents the developed set for evaluation of results. To test the proposed method, at least two separate sets are required for exchange and utilization of data.

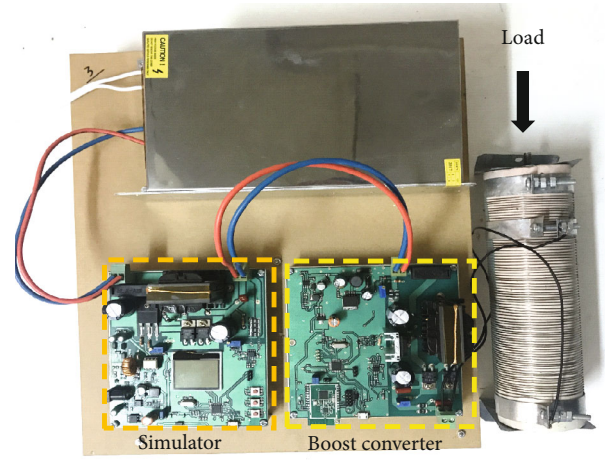

Figure 17: The set of converter and simulator.

5. Results

5.1. Simulation. The PV simulation and proposed algorithm are carried out using MATLAB/SIMULINK. The MPPT process was executed using PSO. The PSC detection, and all mentioned failure modes, has been simulated. It should be noted that when a semiconductor fails, it will be shorted [35–38]. Failures are including:

(a) The converter diode failure

(b) The MOSFET failure used in converter

(c) The panel and its bypass parallel diode disconnection

(d) The panel's bypass parallel diode failure

(e) A panel failure

Figure 18 shows the radiation conditions of panel 3. At the beginning, the radiation value is $1000w/m^2$. Then, it has changed to $600w/m^2$ in second 0.2. In second 0.4, it has changed to $700w/m^2$, and in second 0.7, again it has reached to $1000w/m^2$. These radiation changes only occur in panel 3, meaning that PSC occurs only in panel 3 of PV1, and in other panels, the radiation is equal to $1000w/m^2$.

Figures 19–21 show the voltage, current, and PV1 output power, respectively, and Figures 22–24 show the voltage, current, and PV2 output power, respectively.

From Figures 19 and 22, it can be seen that in different radiations, the output voltages are almost the same, and as the radiation changes, the output current changes.

Figure 25 identifies the PSC. When the output is equal to 1, it means that PSC has been detected and while the output is zero means that PSC has not been detected.

It should be mentioned that here $dP_{\max} = 100w$. Thus, since seconds 0.4 to 0.7, despite a decrease in radiation, PSC is not detected as power difference is lower than $dP_{\max}$. The $dP_{\max}$ can be considered lower to detect even

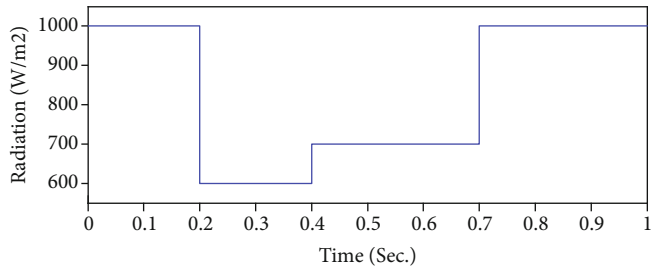

Figure 18: The radiation conditions of panel 3.

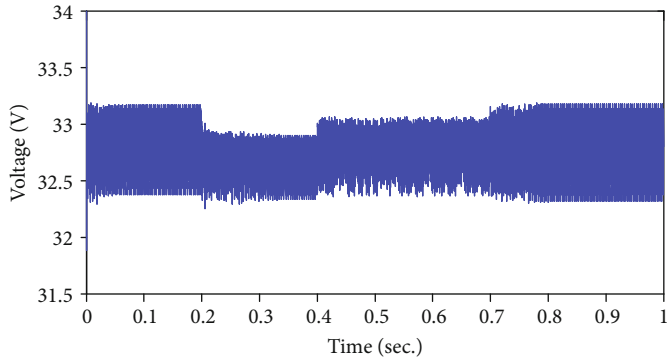

Figure 19: Voltage of PV1.

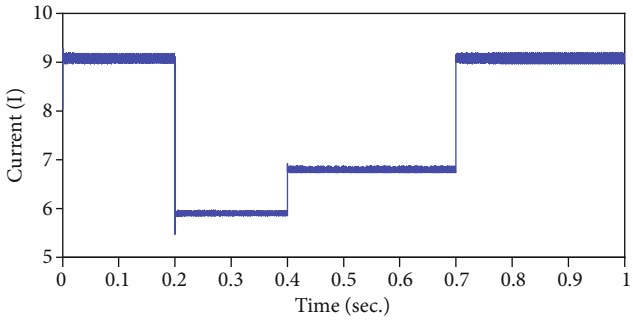

Figure 20: Current of PV1.

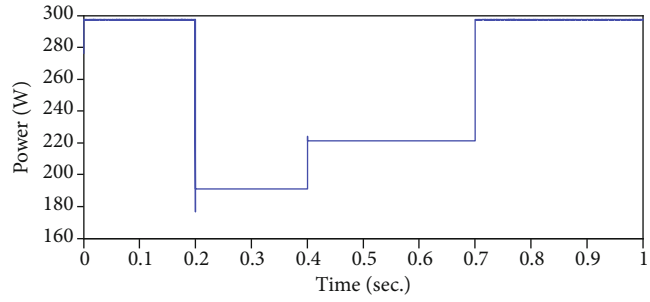

Figure 21: Output power of PV1.

lower power differences. Generally, $dP_{\max}$ is dependent on ambiance condition, maintenance costs, and power requirements.

The radiations in Table 2 are correspondence with the radiation conditions of PV1 panel 3. Figure 26 shows the disconnection moment of panel 3 and the relevant bypass diode. Here, the output voltage and the output power of PV1 are equal to zero, respectively. As shown in Figure 26, after the fault detection, the flag of panel and its bypass diode disconnectivity becomes one.

Figure 27 shows the output voltage of PV1 and PV2, while one of the PV1 panels' is failed. Note the output voltage, which is equal to the sum of the two panel voltage plus the 0.55 of diode voltage. Figure 28 also shows the output voltage of PV1 in detail, while one of panels' is failed.

Figure 29 shows the output voltage of PV1 and PV2, when the PV1 bypass diode of panel 3 has failed. When the bypass diode fails, the circuit is shorted and the output voltage of PV1 will be almost equal to $2/3PV2$. When an error occurs, the related flag becomes 1. Figure 30 shows the output voltage of PV1 in detail, when the bypass diode of panel 3 has failed.

Figure 31 shows the output voltage of PV1, when the MOSFET of converter 1 fails. When the MOSFET fails, the drain-source is shorted and the PV1 output voltage will be zero.

As described in the previous section, when the converter diode fails, the circuit is shorted. If the switch is on, the output voltage of the converter is zero, and if the switch is off, the output voltage of the converter will be equal to its input

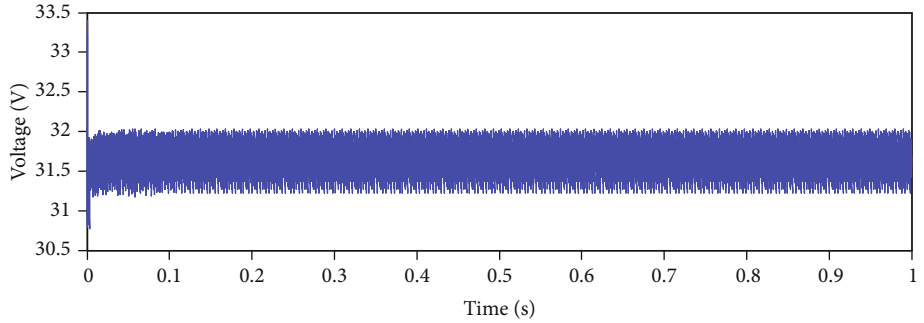

Figure 22: Voltage of PV2.

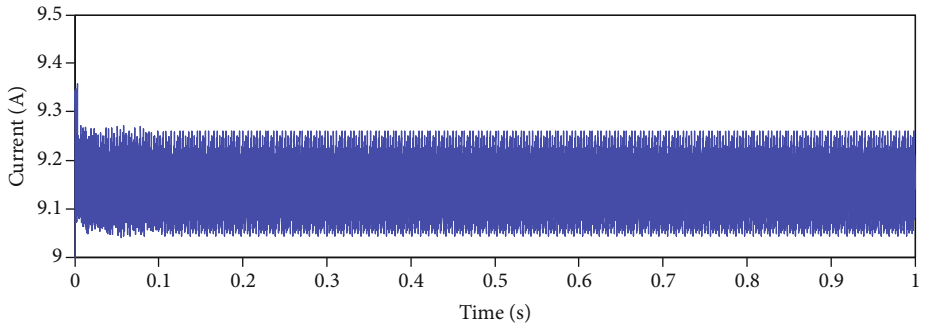

Figure 23: Current of PV2.

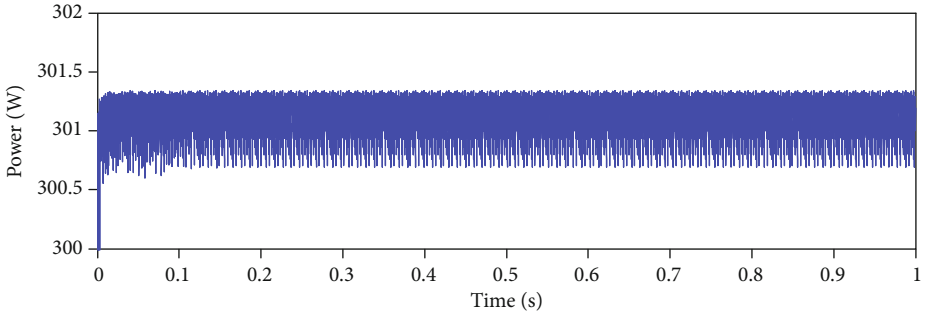

Figure 24: Output power of PV2.

voltage, and the converter will practically fail. Figure 32 shows the converter output voltage when the switch is operating with duty cycle = 10%.

5.2. Experimental. In the first step, the data transmission is studied without MPPT implementation. To this end, a given set of data is exchanged between two sets.

To study the detection of partial shading, two simulators and two converters are used. One simulator was regulated for uniform radiation, and the other was programmed such that, after a given time interval, it changed from uniform radiation to partial shading on the panel assuming 1000 W/m^2 irradiance for two-thirds of the panel area and variable irradiation for the remaining one-third as shown in Figure 33.

Figure 34 shows the voltage-power curve corresponding to the three cases discussed above. The values of voltage, current, and power for panel 1 are shown in Figures 35–37, respectively; whereas the corresponding values for panel 2 are shown in Figures 38–40, respectively.

As expected, the current and power for panel 1 changed with the radiation level, while they remained constant for panel 2 due to constant radiation levels.

As it can be seen in Figure 33, 0.2 seconds after conditions are changed and after a reassessment of conditions, the variable corresponding to the partial shading readjusts

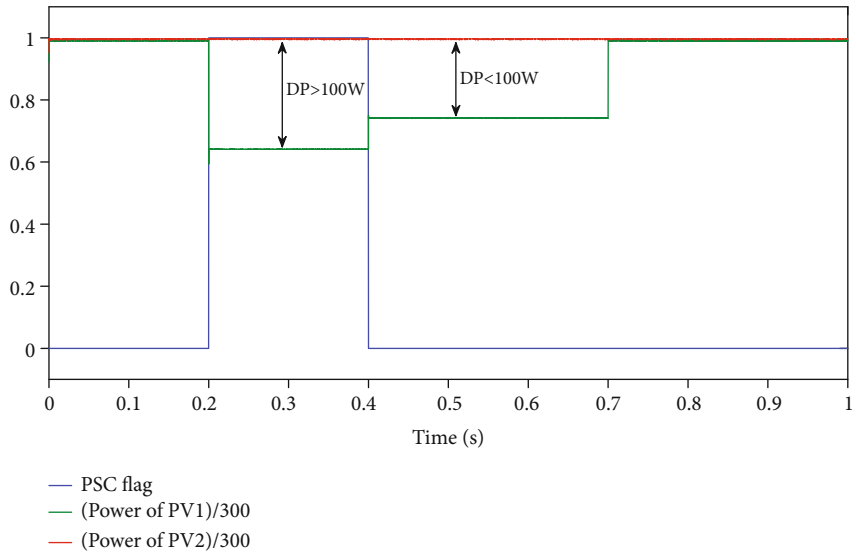

Figure 25: Partial shading condition detection.

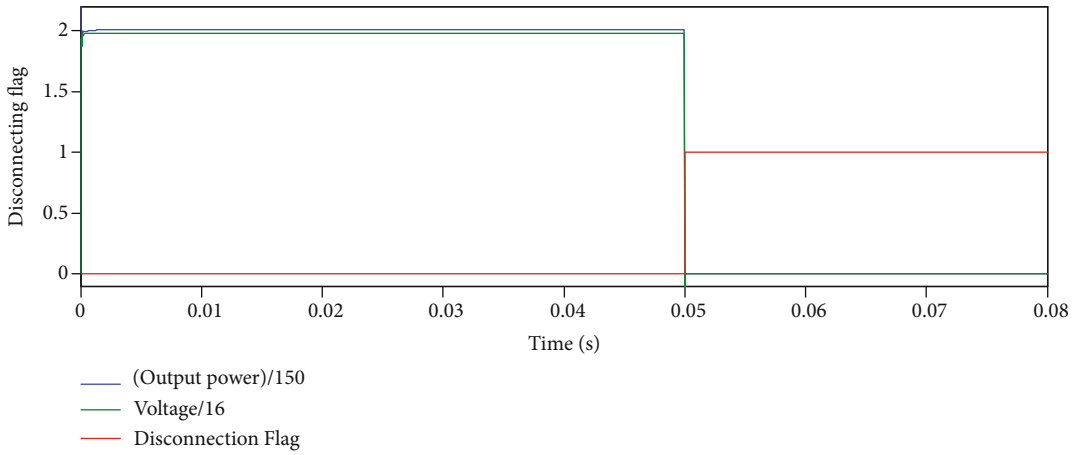

Figure 26: Panel 3 and the relevant bypass diode disconnection fault.

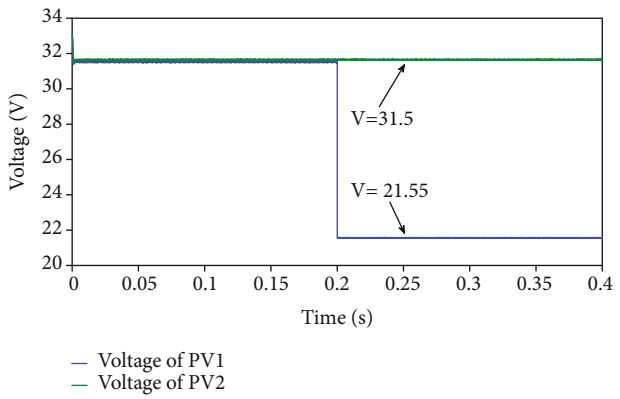

Figure 27: The output voltage of PV1 and PV2, while one of the PV1 panels' is failed.

to implement the bypass algorithm. After the implementation is done, this variable is reset as to prevent any problem for the process to continue.

Figures 34–47 show the experimental results. It is worth mentioning that all of the measured parameters belong to the output of PVs, not the output of converter.

Power curves for panels 1 and 2 are shown on the same graph in Figure 41. At the instant of radiation change, i.e., 0.2 s, a significant change is observed between the two curves, indicating partial shading over the panel with reduced power, leading to the radiation detection flag being triggered, and running the algorithm to find the point of maximum power under partial shadow conditions. This flag is shown in Figure 42.

In order to detect the panel faults, one of the simulators was programmed in the constant radiation mode; while the other was programmed so as to simultaneously set its voltage and power equal to zero at a specific instant, which

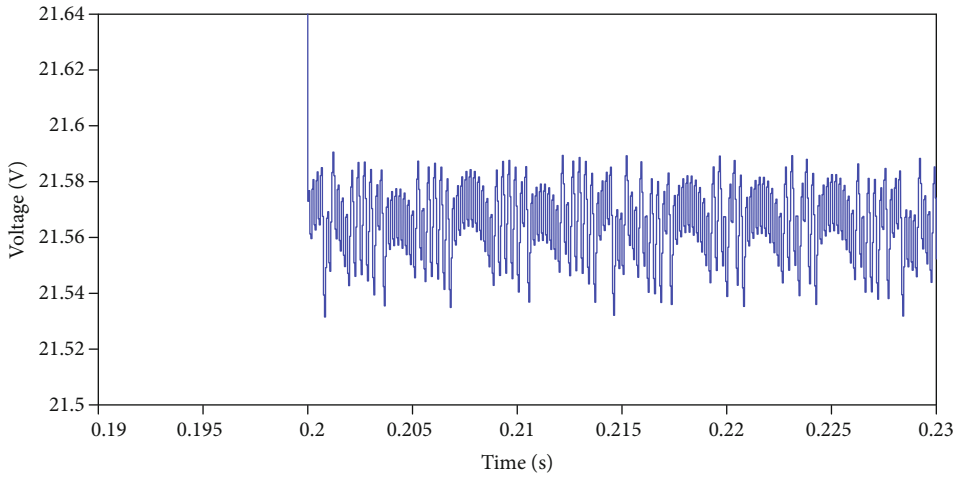

Figure 28: The output voltage of PV1, while one of panels' is failed.

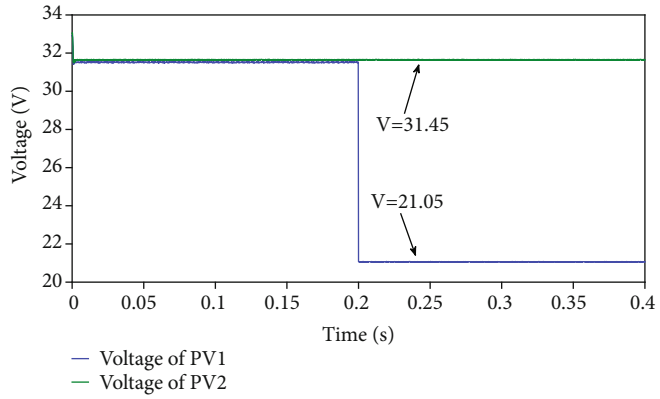

Figure 29: The output voltage of PV1 and PV2, when the bypass diode of panel 3 has failed.

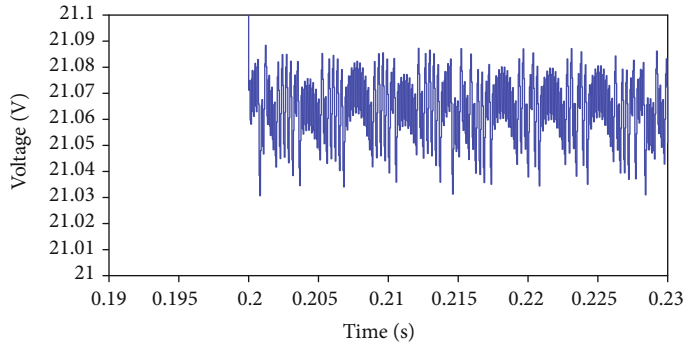

Figure 30: The output voltage of PV1 in detail, when the bypass diode of panel 3 has failed.

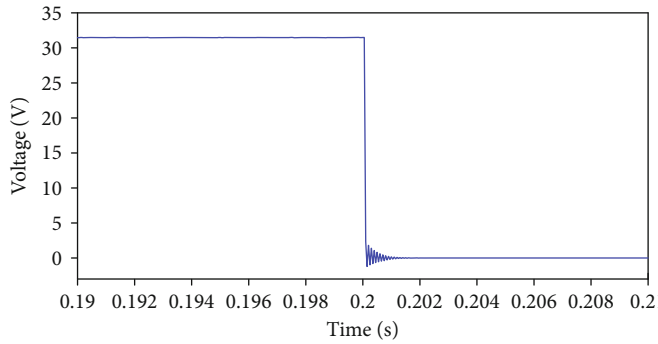

Figure 31: The output voltage of PV1, when the MOSFET of converter 1 fails.

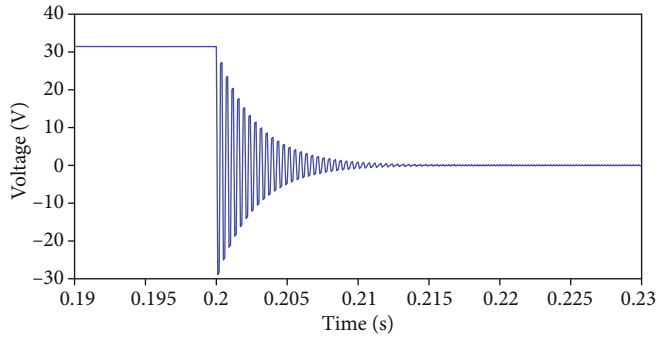

Figure 32: The converter output voltage, when its diode fails.

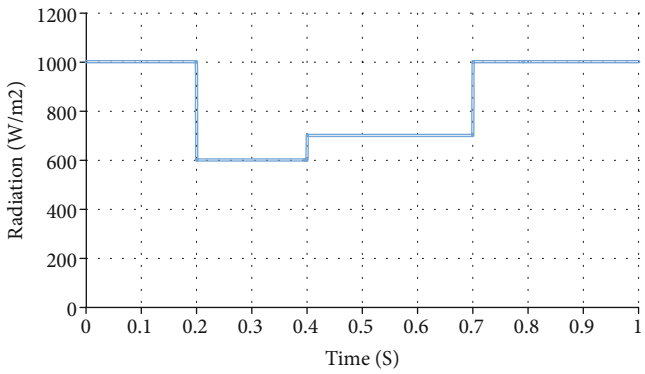

Figure 33: The radiation of partial shading condition.

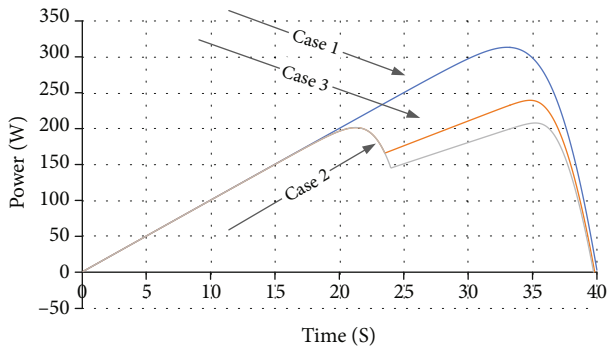

Figure 34: The power-voltage characteristics of PV simulator on different PSCs.

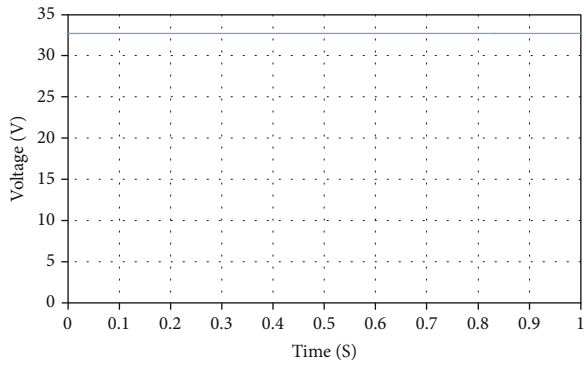

Figure 35: The output voltage of PV1.

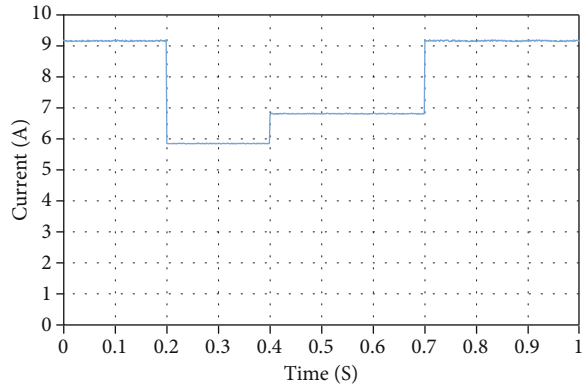

Figure 36: The output current of PV1.

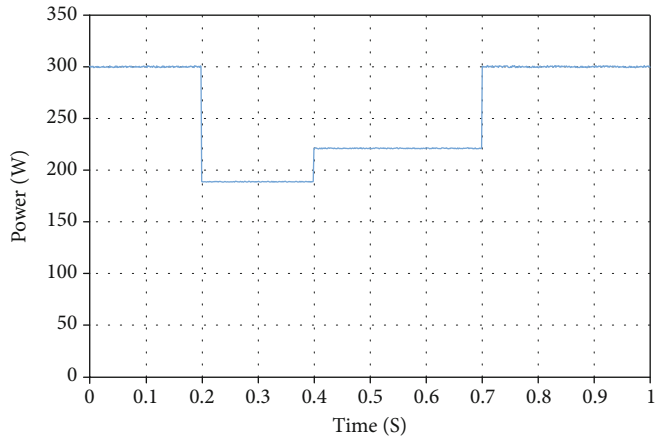

Figure 37: The output power of PV1.

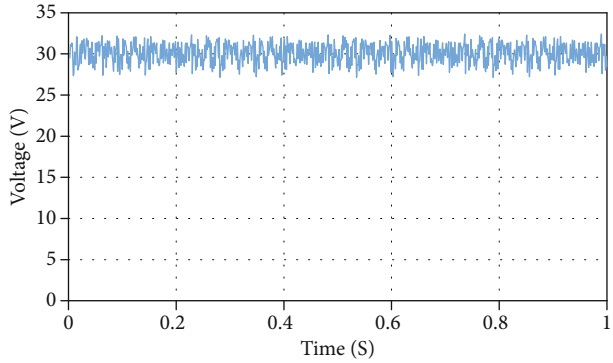

Figure 38: The output voltage of PV2.

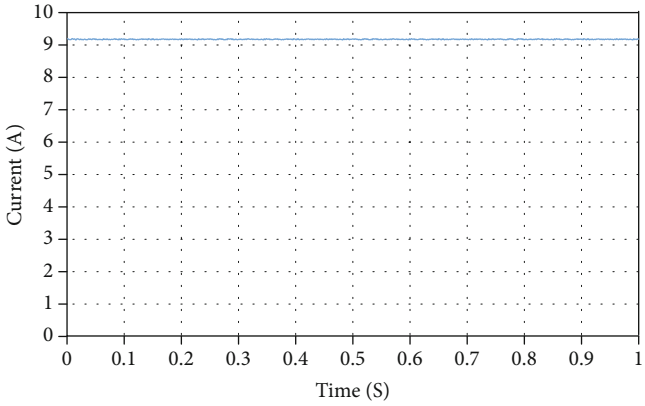

Figure 39: The output current of PV2.

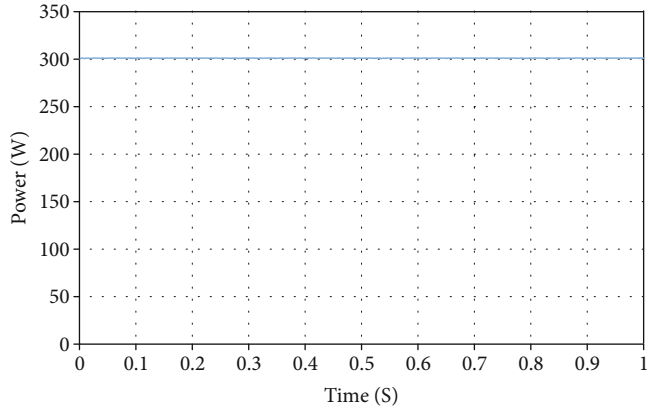

Figure 40: The output power of PV2.

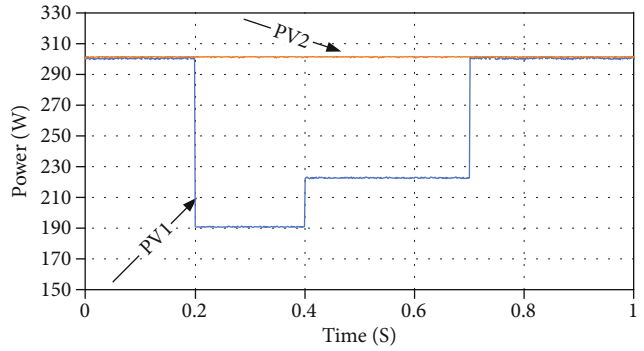

Figure 41: Compare of PV1 and PV2 output powers.

simulated panel disconnection and panel bypass diode short circuit. To better illustrate the details, the voltage and power of the simulator with the fault are shown in Figure 43 at ratios 1/16 and 1/50, respectively. It is observed that the fault was detected by considering the power generated by the simulator that had no faults and the sudden reduction of the power and voltage of the other simulator to zero, triggering the respective flag and detecting the fault.

If one or both of the strings constituting the panel experience a problem, the panel voltage is relatively reduced, which can be used in the detection of string disconnection. Figures 44 and 45 show the conditions for disconnection of one and two strings, respectively.

This system can also detect some other converter issues such as diode and switch faults. Experimental analysis of these faults requires a converter that can simulate them.

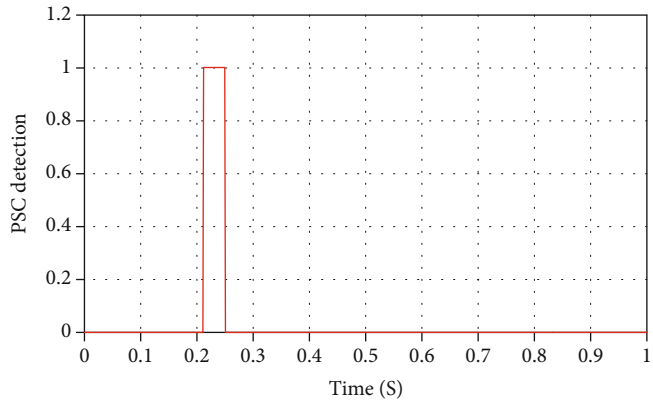

Figure 42: The PSC detection flag.

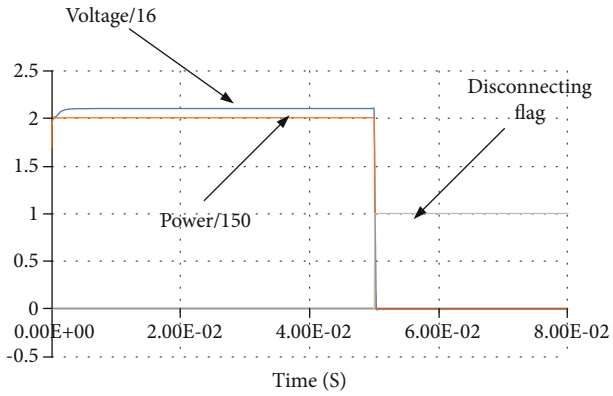

Figure 43: Disconnecting flag of a panel and its relevant bypass diode.

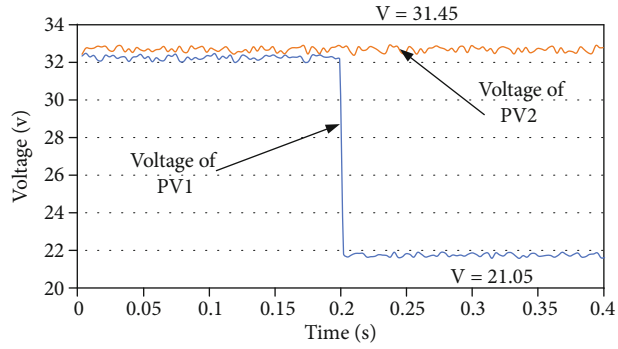

Figure 45: The output voltage of PV1 and PV2, when the bypass diode of panel 3 has failed.

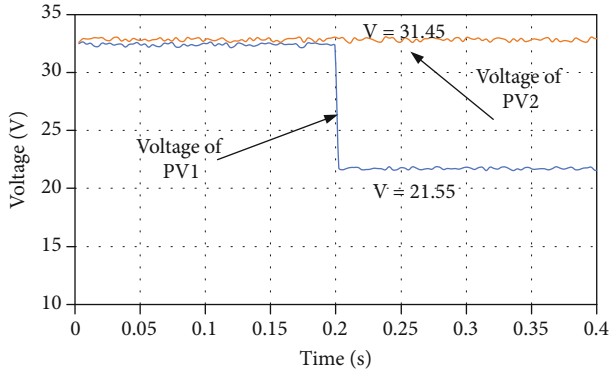

Figure 44: The output voltage of PV1 and PV2, while one of the PV1 panels' is failed.

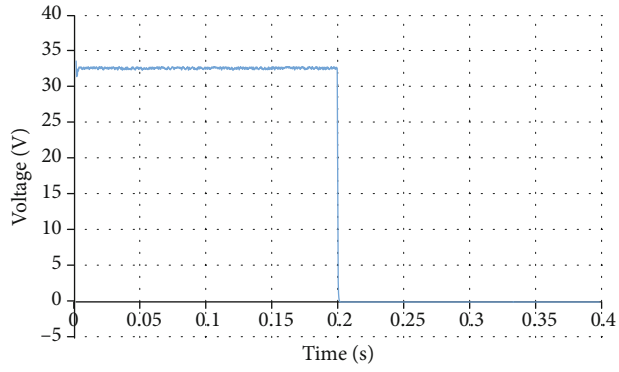

Figure 46: The output voltage of PV1, when the MOSFET of converter 1 fails.

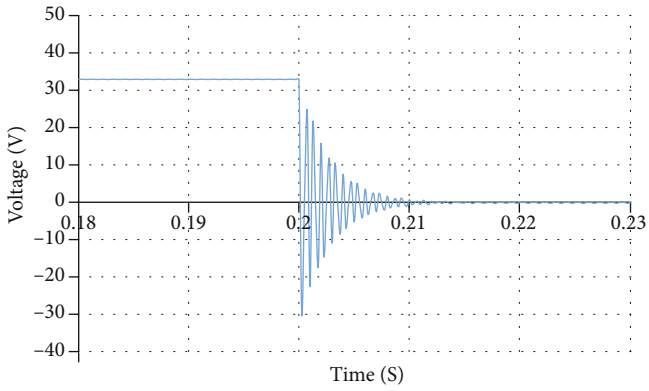

Figure 47: Detection of converter diode failure.

Since the research group did not have access to such a converter, this capability was analyzed only through simulations, whose results are presented in Figures 46 and 47.

6. Conclusion

In a photovoltaic system, it is vital to accurately identify the partial shading condition of a panel; however, sometimes a fault might be confused with the partial shading condition. In this paper, a novel algorithm for diagnosing, partial shading condition, and fault detection in a practical and uncomplicated way in a domestic photovoltaic system is presented. The faults that may occur in converters and photovoltaic panels were investigated, and methods for detecting them from each other were introduced. The domestic network is composed of two adjacent identical photovoltaic systems, employing three series panels. The proposed algorithm detects fault and PSC by comparing the photovoltaic system parameters with each other. MPPT was also performed by PSO method. The simulations were carried out in MATLAB/SIMULINK software and then in a real network. The Zigbee protocol was also chosen to data exchange of converters.

The main results of the present work are

(i) The existing results indicated the applicability, high accuracy, and speed of the proposed method in diagnosing and detection fault and partial shading condition

(ii) The simulation and laboratory results were similar in identification of the event of partial shadow using the innovative method of comparison of electric parameters of adjacent panels. The results were suggestive of the correct performance of the designed system

(iii) Diagnosis of some panel errors was performed by comparing the electric parameters of adjacent panels, and the results from the simulation and experiment validated our choice of method

(iv) Diagnosis of some of converter errors such as diode failure and switch problems was performed by analyzing the entire information of the network, and the simulation results were indicative of detection of these errors using the proposed method

In addition to partial shading and fault detection, the data exchange link can also be used for implementation of an integrated management system for solar domestic-purpose systems.

Data Availability

Data is available on request.

Conflicts of Interest

The authors declare that they have no conflicts of interest.

References

[1] S. W. Blume, "Generation," in *Electric Power System Basics for the Nonelectrical Professional*, pp. 19–41, 2017.

[2] M. Mohamed, A. A. Zaki Diab, and H. Rezk, "Partial shading mitigation of PV systems via different meta-heuristic techniques," *Renewable Energy*, vol. 130, pp. 1159–1175, 2019.

[3] P. Bharadwaj and V. John, "Subcell modeling of partially shaded photovoltaic modules," *IEEE Transactions on Industry Applications*, vol. 55, no. 3, pp. 3046–3054, 2019.

[4] Z. Bi, J. Ma, K. Wang, K. Man, J. Smith, and Y. Yue, "Identification of partial shading conditions for photovoltaic strings," *IEEE Access*, vol. 8, pp. 75491–75502, 2020.

[5] J. Ma, H. Jiang, Z. Bi, K. Huang, X. Li, and H. Wen, "Maximum power point estimation for photovoltaic strings subjected to partial shading scenarios," *IEEE Transactions on Industry Applications*, vol. 55, no. 2, pp. 1890–1902, 2019.

[6] M. Arjun, V. Ramana, R. Viswadev, and B. Venkatesaperumal, "An iterative analytical solution for calculating maximum power point in photovoltaic systems under partial shading conditions," *IEEE Transactions on Circuits and Systems II: Express Briefs*, vol. 66, no. 6, pp. 973–977, 2019.

[7] N. Priyadarshi, "Practical realization of an improved photovoltaic grid integration with MPPT," *International journal of renewable energy research*, vol. 7, pp. 1880–1891, 2017.

[8] N. Priyadarshi, A. Sharma, and S. Priyam, "An experimental realization of grid-connected PV system with MPPT using dSPACE DS 1104 control board," in *Advances in Smart Grid and Renewable Energy*, S. SenGupta, A. Zobaa, K. Sherpa, and A. Bhoi, Eds., vol. 435 of Lecture Notes in Electrical Engineering, Springer, Singapore, 2018.

[9] K. Hu, S. Cao, W. Li, and F. Zhu, "An improved particle swarm optimization algorithm suitable for photovoltaic power tracking under partial shading conditions," *IEEE Access*, vol. 7, pp. 143217–143232, 2019.

[10] N. Priyadarshi, S. Padmanaban, P. Kiran Maroti, and A. Sharma, "An extensive practical investigation of FPSO-Based MPPT for grid integrated PV system under variable operating conditions with Anti-Islanding protection," *IEEE Systems Journal*, vol. 13, no. 2, pp. 1861–1871, 2019.

[11] N. Priyadarshi, S. Padmanaban, J. Holm-Nielsen, F. Blaabjerg, and M. S. Bhaskar, "An experimental estimation of hybrid ANFIS–PSO-Based MPPT for PV grid integration under fluctuating sun irradiance," *IEEE Systems Journal*, vol. 14, no. 1, pp. 1218–1229, 2020.

[12] N. Priyadarshi, A. Anand, A. Sharma, F. Azam, V. Singh, and R. Sinha, "An experimental implementation and testing of GA based maximum power point tracking for PV system under varying ambient conditions using dSPACE DS 1104 controller," *International Journal of Renewable Energy Research*, vol. 7, pp. 255–265, 2017.

[13] N. Priyadarshi, A. K. Sharma, and F. Azam, "A hybrid firefly-asymmetrical fuzzy logic controller based MPPT for PV -wind-fuel grid integration," *International Journal of Renewable Energy Research*, vol. 7, pp. 1546–1560, 2017.

[14] P. Sanjeevikumar, N. Priyadarshi, J. Holm-Nielsen et al., "A novel modified sine-cosine optimized MPPT algorithm for grid integrated PV system under real operating conditions," *IEEE Access*, vol. 7, pp. 10467–10477, 2019.

[15] J. Ahmed and Z. Salam, "An accurate method for MPPT to detect the partial shading occurrence in a PV system," *IEEE Transactions on Industrial Informatics*, vol. 13, no. 5, pp. 2151–2161, 2017.

[16] K. Kaced, C. Larbes, N. Ramzan, M. Bounabi, and E. Dahmane, "Bat algorithm based maximum power point tracking for photovoltaic system under partial shading conditions," *Solar Energy*, vol. 158, pp. 490–503, 2017.

[17] K. Ishaque, Z. Salam, H. Taheri, and Syafaruddin, "Modeling and simulation of photovoltaic (PV) system during partial shading based on a two-diode model," *Simulation Modelling Practice and Theory*, vol. 19, no. 7, pp. 1613–1626, 2011.

[18] C. Correa-Betanzo, H. Calleja, C. Aguilar, A. López Núñez, and E. Rodriguez, "Photovoltaic-based DC microgrid with partial shading and fault tolerance," *Journal of Modern Power Systems and Clean Energy*, vol. 7, no. 2, pp. 340–349, 2019.

[19] D. Gokilapriya and S. Banu, "MPPT measurement of photovoltaic system under partial shading condition using DPSO algorithm," in *Power Electronics and Renewable Energy Systems*, C. Kamalakannan, L. Suresh, S. Dash, and B. Panigrahi, Eds., vol. 326 of Lecture Notes in Electrical Engineering, Springer, New Delhi, 2015.

[20] J. Farzaneh, R. Keypour, and M. A. Khanesar, "A new maximum power point tracking based on modified firefly algorithm for PV system under partial shading conditions," *Technology and Economics of Smart Grids and Sustainable Energy*, vol. 3, no. 1, 2018.

[21] S. Vijayalekshmy, S. Iyer, and B. Beevi, "Comparative analysis on the performance of a short string of series-connected and parallel-connected photovoltaic array under partial shading," *Journal of The Institution of Engineers (India): Series B*, vol. 96, no. 3, pp. 217–226, 2014.

[22] D. Martin, J. R. Vazquez, and J. M. Cano, "MPPT in PV systems under partial shading conditions using artificial vision," *Electric Power Systems Research*, vol. 162, pp. 89–98, 2018.

[23] D. S. Pillai, F. Blaabjerg, and N. Rajasekar, "A comparative evaluation of advanced fault detection approaches for PV systems," *IEEE Journal of Photovoltaics*, vol. 9, no. 2, pp. 513–527, 2019.

[24] N. Ghaffarzadeh and A. Azadian, "A comprehensive review and performance evaluation in solar (PV) systems fault classification and fault detection techniques," *Journal of solar energy Research*, vol. 4, no. 4, pp. 252–272, 2019.

[25] A. Chouder and S. Silvestre, "Automatic supervision and fault detection of PV systems based on power losses analysis," *Energy Conversion and Management*, vol. 51, no. 10, pp. 1929–1937, 2010.

[26] D. S. Pillai and N. Rajasekar, "An MPPT based sensorless line-line and line-ground fault detection technique for PV systems," *IEEE Transactions on Power Electronics*, vol. 34, no. 9, pp. 8646–8659, 2018.

[27] E. Jamshidpour, P. Poure, and S. Saadate, "Common switch fault diagnosis for two-stage DC-DC converters used in energy harvesting applications," *Electronics*, vol. 8, no. 3, p. 293, 2019.

[28] I. U. Khalil, A. Ul-Haq, Y. Mahmoud et al., "Comparative analysis of photovoltaic faults and performance evaluation of its detection techniques," *IEEE Access*, vol. 8, pp. 26676–26700, 2020.

[29] M. W. Ahmad, N. B. Y. Gorla, H. Malik, and S. K. Panda, "A fault diagnosis and postfault reconfiguration scheme for interleaved boost converter in PV-based system," *IEEE Transactions on Power Electronics*, vol. 36, no. 4, pp. 3769–3780, 2021.

[30] I. Zurbriggen and M. Ordonez, "PV energy harvesting under extremely fast changing irradiance: state-plane direct MPPT," *IEEE Transactions on Industrial Electronics*, vol. 66, no. 3, pp. 1852–1861, 2019.

[31] H. A. Raeisi and S. M. Sadeghzadeh, "Designing and construction of a solar panel simulator capable of simulating partial shading conditions," *Journal of Solar Energy Research*, vol. 4, no. 1, pp. 15–21, 2019.

[32] A. Elserougi, M. Diab, A. Massoud, A. Abdel-Khalik, and S. Ahmed, "A switched PV approach for extracted maximum power enhancement of PV arrays during partial shading," *IEEE Transactions on Sustainable Energy*, vol. 6, no. 3, pp. 767–772, 2015.

[33] T. Zouaghi and M. Poloujadoff, "Modeling of polyphase brushless exciter behavior for failing diode operation," *IEEE Transactions on Energy Conversion*, vol. 13, no. 3, pp. 214–220, 1998.

[34] A. Fitzgerald, ""A fail-safe" circuit principle in semiconductor and solid-state systems," *IEEE Transactions on Magnetics*, vol. 2, no. 1, pp. 35–38, 1966.

[35] S. Sleva and Y. Taur, "The influence of source and drain junction depth on the short-channel effect in MOSFETs," *IEEE Transactions on Electron Devices*, vol. 52, no. 12, pp. 2814–2816, 2005.

[36] R. van Langevelde and F. M. Klaassen, "Effect of gate-field dependent mobility degradation on distortion analysis in MOSFETs," *IEEE Transactions on Electron Devices*, vol. 44, no. 11, pp. 2044–2052, 1997.

[37] J. Xue, Z. Xin, H. Wang, P. C. Loh, and F. Blaabjerg, "An Improveddi/dt-RCD Detection for short-circuit protection of SiC mosfet," *IEEE Transactions on Power Electronics*, vol. 36, no. 1, pp. 12–17, 2021.

[38] J. J. Barnes, K. Shimohigashi, and R. W. Dutton, "Short-channel MOSFETs in the punchthrough current mode," *IEEE Journal of Solid-State Circuits*, vol. 14, no. 2, pp. 368–375, 1979.